International Journal of Pharmaceutics 599 (2021) 120417

Contents lists available at ScienceDirect

International Journal of Pharmaceutics

journal homepage: www.elsevier.com/locate/ijpharm

Development of immediate release 3D-printed dosage forms for a poorly water-soluble drug by fused deposition modeling: Study of morphology, solid state and dissolution

Marina Fanous [a,b], Malak Bitar [a], Sarah Gold [a], Adam Sobczuk [a], Stefan Hirsch [a], Joerg Ogorka [a], Georgios Imanidis [b,c,*]

[a] Novartis Pharma AG, Basel, Switzerland
[b] Department of Pharmaceutical Sciences, University of Basel, Basel, Switzerland
[c] School of Life Sciences, University of Applied Sciences Northwestern Switzerland, Muttenz, Switzerland

ARTICLE INFO

Keywords:
3D-printing
Tablet
Immediate release
Poorly soluble drug
X-ray computer microtomography
Personalized dosage form
BCS class IV drug

ABSTRACT

3D-printing technologies such as Fused Deposition Modeling (FDM) bring a unique opportunity for personalized and flexible near-patient production of pharmaceuticals, potentially improving safety and efficacy for some medications. However, FDM-printed tablets often exhibit tendency for slow dissolution due to polymer erosion-based dissolution mechanisms. Development of immediate release (IR) 3D-printed dosage with poorly water-soluble compounds is even more challenging but necessary to ensure wide applicability of the technology within pharmaceutical development portfolios. In this work, process and morphology were considered to achieve IR of BCS class IV compound lumefantrine as model active pharmaceutical ingredient (API) using basic butylated methacrylate copolymer (Eudragit EPO) as matrix former, as well as hydrophilic plasticizer xylitol and pore former maltodextrin. Grid-designed tablets with size acceptable for children from 6 years old and varying programmed infill density were successfully 3D-printed with 5% lumefantrine while higher drug load led to increased brittleness which is incompatible with 3D-printing. Lumefantrine assay was 92 to 97.5% of theoretical content depending on drug load and process parameters. 3D-printed tablets with 65% infill density met rapid release criteria, while 80% and 100% showed slower dissolution. Structural characteristics of 3D-printed tablets with non-continuous surface such as accessible porosity and specific surface area by weight and by volume were quantified by a non-destructive automated μCT-based methodology and were found to correlate with dissolution rate. Increase in accessible porosity, total surface area, specific surface area and decrease in relative density were statistically significant critical factors for modification of lumefantrine dissolution rate. Crystallinity in manufactured tablets and filaments was explored by highly sensitive Raman mapping technique. Lumefantrine was present in the fully amorphous state in the tablets exhibiting adequate stability for on-site manufacturing. The study demonstrates feasibility of immediate release FDM-3D-printed tablets with BCS class IV API and illustrates the correlation of FDM design parameters with morphological and dissolution characteristics of manufactured tablets.

1. Introduction

3D-printing of pharmaceuticals could improve individualization of drug therapy through personalized dosage strengths (Norman et al., 2017), which has the potential to improve safety and efficacy for some medications (NHS, 2016; Vogenberg et al., 2010). Solid dosage forms of various designs, fabricated through layer-by-layer addition of materials based on a digital model can be created via numerous 3D-printing technologies (Kyobula et al., 2017). Further, manufacturing of drug products at hospitals and pharmacies with multiple active pharmaceutical ingredients (APIs) and tailored release profiles, possibly involving complex designs and geometries, might enable pharmaceutical 3D-printing to fulfil as yet unmet clinical needs (Awad et al., 2020, 2019; Rycerz et al.. 2019).

* Corresponding author at: School of Life Sciences, University of Applied Sciences Northwestern Switzerland, Hofackerstrasse 30, 4132 Muttenz/Basel, Switzerland.
E-mail address: georgios.imanidis@unibas.ch (G. Imanidis).

https://doi.org/10.1016/j.ijpharm.2021.120417
Received 24 November 2020; Received in revised form 18 February 2021; Accepted 19 February 2021
Available online 27 February 2021

Fused Deposition Modeling (FDM) 3D-printing brings a unique opportunity for flexible and personalized production of pharmaceuticals (Norman et al., 2017; Trenfield et al., 2018). For FDM, a thermoplastic filament obtained via hot-melt extrusion, is deposited in ultrafine threads through the printhead nozzle (Ilyés et al., 2019). This technology could be advantageous for dosage forms manufacturing via low-cost FDM 3D-printers in clinical settings and decentralized locations as no powder or solvents (Zema et al., 2017) are involved in the printing process, post-processing maybe avoided and mechanically strong tablets are produced (Pietrzak et al., 2015). In addition, different dosage strengths with a variety of drug release profiles were delivered within certain limits from the same filament (Arafat et al., 2018). The challenges to overcome are risk of thermal degradation during processing (Goyanes et al., 2014a) and FDM processability dependent on mechanical properties of the filament (Alhnan et al., 2016). Moreover, FDM-tablets often show tendency for slow dissolution due to the active pharmaceutical ingredient (API) being enclosed by polymeric matrices characterized by erosion-controlled dissolution mechanism (Goyanes et al., 2014b). Most of the developed formulations for FDM exhibit slow release even for hydrophilic model drug substances embedded in water-soluble polymers (Arafat et al., 2018; Azad et al., 2020; Curti and Russell, 2020; Goyanes et al., 2014a, 2016; Ilyés et al., 2019). Development of immediate release (IR) dosage forms is more demanding (Solanki et al., 2018; Wei et al., 2020), yet necessary if the technology is to be applied commercially (GBIResearch, 2012; Marketsandmarkets, 2013). This limitation is particularly critical for poorly water-soluble drugs, belonging to Biopharmaceutics Classification System (BCS) classes II and IV. For orally administered compounds with dissolution-limited absorption (Butler, 2010) even a small increase in dissolution rate sometimes results in large increase of bioavailability (Lobenberg, 2000). Development of rapidly dissolving 3D-printed tablets for lipophilic compounds, therefore, is a clear need towards the future of personalized dosage form production, since majority of discovered drug candidates exhibit poor aqueous solubility (Boyd et al., 2019; Kawabata et al., 2011).

To overcome incomplete bioavailability, dissolution rate of FDM 3D-printed tablets could be improved via design modification, i.e. lowering infill density without changing formulation composition (Arafat et al., 2018; Korte, 2018), as opposed to standard dosage forms often necessitating changes in formulation possibly resulting in incompatibility and stability issues. It is known, for instance, that decrease in programmed infill density often accelerates drug dissolution rate for both lipophilic (Solanki et al., 2018) and hydrophilic drugs (Fanous et al., 2020b), yet very few studies have explored how programmed structure is translated into actual morphology. The micropore volume measured by destructive mercury porosimetry, for example, did not correlate with dissolution profile of caffeine/paracetamol from polyvinyl alcohol (PVA)-based 3D-printed tablets with 100% programmed infill density (Goyanes et al., 2016). The authors concluded that porosity was not predictive of drug release possibly due to the swelling of PVA. The same group pioneered the study of the effect of 3D-printed tablet geometry (cube, pyramid, cylinder, sphere and torus) on drug dissolution rate (Goyanes et al., 2015) and found that geometrical shape affected release of a model API dependent on surface area-to-volume ratio (Goyanes et al., 2015). However, precision of manual measurements of dimensions was limited and tablet designs with infill density lower than 100% were not addressed.

Non-destructive X-ray microcomputer tomography (μCT) to explore effect of surface area on dissolution rate of Eudragit RL-based tablets was used (Korte, 2018). Specific surface area of the internal network of the tablets hardly varied with changing infill density and a slower drug dissolution for dosage forms with a denser network was found which was attributed to restricted perfusion of the dosage form by the medium. Other authors designed 3D-printed tablets consisting of blocks and bridges with gaps in-between (Arafat et al., 2018). *In-vitro* drug release rate was directly related to the distance between the structural blocks whereas accelerating drug release and achieving immediate release properties was primarily connected to breakage of tablets into smaller structures. Dissolution rate, however, did not correlate with surface area-to-mass ratio measured by μCT and the size of 3D-printed tablets was large potentially limiting patient acceptability. Hence, defining key design parameters impacting dissolution rate and understanding the link between intended and realized morphology are still open issues in FDM 3D-printed tablets. Also, in all hitherto studies, μCT image post processing outcome was not verified in providing accurate estimate of virtual 3D-morphometry values and did not address the level of 3D shape descriptors.

Understanding how 3D-printing process and design characteristics influence the variety of structural factors such as relative density, volume of accessible and closed pores, surface area, volume of solid polymer matrix, and how these in turn affect dissolution profile is crucial towards tailoring desired release profile. Moreover, as FDM 3D-printing is in essence a hot-melt extrusion process, its role for solid state transformation potentially affecting dissolution of the API has to be addressed. The objectives of this study therefore were:

- Develop immediate release (IR) FDM 3D-printed dosage forms with a size suitable also for pediatric population above the age of 6 years with a BCS class IV model compound
- Precisely quantify the morphological characteristics of the manufactured 3D-printed tablets by developing automated non-destructive, imaging based, analytical methodology based on μCT and analyze API solid state in filaments and in tablets by highly sensitive confocal Raman microscopy
- Bridge between programmed and actual structure of tablets with several designs and evaluate specific surface area accessible for dissolution and pore volume for identifying structural parameters that are responsible for dissolution rate acceleration

This study involves formulation, process, and structure design for 3D-printed dosage forms to achieve immediate release with the BCS IV model compound lumefantrine. Basic butylated methacrylate copolymer (Eudragit EPO) was chosen as matrix former, since methacrylates have shown potential to achieve IR (Sadia et al., 2016; Sadia et al., 2018) and ability to form amorphous solid dispersion with lumefantrine (Jain et al., 2018; Meier et al., 2008; Song et al., 2016). Hydrophilic plasticizer xylitol and pore former maltodextrin were selected as promising combination to achieve rapid dissolution (Fanous et al., 2020a; Puri et al., 2017). FDM tablets were manufactured above melting temperature of API, with infill density between 65 and 100%. Although lumefantrine might require chemical stabilizer/antioxidant in the formulation (Jain et al., 2018), such additives were not used in this study in order to gain an insight into the effect of hot-melt extrusion and 3D-printing on stability of this compound. Few examples of FDM 3D-printed IR tablets with poorly water-soluble API and of bridging between designed and actual morphological product parameters have been reported, while the newly developed μCT- and Raman-based methodologies have not been used in this context before.

2. Materials and methods

2.1. Materials

Lumefantrine (Novartis Pharma AG, Switzerland), molecular weight 528.9 g/mol, was used as a model compound. Powder mixtures of basic butylated methacrylate copolymer (Eudragit EPO, Evonik, Germany) as primary matrix former, xylitol (Xylisorb300, Roquette, France) as hydrophilic plasticizer and maltodextrin (Maldex 120, Tereos, Germany) as pore former were prepared. Formulations containing increasing concentrations of model drug were hot-melt extruded to produce filaments, whose 3D-printability was assessed. Amorphous lumefantrine (Novartis Pharma AG, Switzerland) was used as a reference for Raman

microscopy. Lumefantrine 120 mg tablets (Novartis Pharma AG, Switzerland) were used for comparison in dissolution studies.

2.2. Methods

2.2.1. Hot-melt extrusion (HME)

Powders were accurately weighed into 0.5 L bottles to make a total batch weight of 100 g and were mixed via diffusion blending for 20 min at 32 Alternrpm by T2 Turbula™ mixer. A twin-screw hot melt extruder (Thermo Scientific™ Pharma 11™, Karlsruhe, Germany) was used for filament manufacturing. The screw design was TIP/10 × FE/4 × 90°/5 × 60°/3 × 30°/25 × FE/1 × ½ FE/FEEDING. A schematic representation was published previously (Fanous et al., 2020a).

Temperature was empirically adjusted to assure steady production of appropriate filaments while torque and pressure were recorded. Measured temperature for zones 2, 3, 4,5–8 was 38–43 °C, 60–80 °C, 100–140 °C, 120–141 °C, respectively; die temperature was 120–142 °C depending on the formulation (see Table 1). Extrusion was carried out through a customized 1.75 mm die nozzle with a pressure control (maximum 90 bar). Feeding rate was about 4 g/min, screw speed 15–27 rpm depending on the formulation (see Table 1 for details).

2.2.2. Fused deposition modeling (FDM) 3D-printing

The template used to print the dosage form was designed with FreeCAD 0.13 software. The selected geometry was an oval tablet with grid infill pattern. The tablet dimensions of 9 × 5 × 4 mm (width × length × height) were selected, with one continuous outer layer (altitude shell) and no continuous bottom/top layers. The continuous outer layer enclosed the perimeter of the structure which had no bottom or top layer. BoltPro 3D-printer (LeapFrog, Netherlands) and the in-built software was used for FDM. 3D-printing was performed through nozzle with d = 0.5 mm at 1000 mm/min speed with primary layer speed of 50% of the default and height of 0.15 mm. The lowest possible printing temperature was used that still allowed an appropriate formulation processability (165 °C for placebo and 160 °C for active formulation). The printing platform was heated to 35 °C during FDM.

Three infill densities were printed: 100%, 80% and 65%. After 3D-printing, the manufactured tablets were weighed (n = 6) and their dimensions were measured (n = 3) manually with a caliper.

2.2.3. Drug load, degradation products and uniformity of percent drug content

A tablet was dissolved in 100 ml of sample solvent (20 mM hexanesulfonic acid: water: acetonitrile: TFA) and the drug concentration was determined by HPLC (HP-1100, Agilent Technologies, UK) with YMC Pack-Pro C-185 μm, 150 × 3 mm column (YMC Co., Japan), maintained at 30 °C. The injected volume was 10 μl. The gradient consisted of two components: mobile phase A (20 mM hexanesulfonic acid: acetonitrile: TFA; 490:510:1, v/v/v) and mobile phase B (acetonitrile: TFA,; 1000:1 v/v) starting with the former at 100% and decreasing gradually to 48% after 16 min, and increasing back to 100% after 20.1 min. The flow rate was 1 ml/min and UV detection was carried out at a wavelength of 265 nm. All measurements were performed in triplicate. To calculate the average percent drug content, values of randomly selected (n = 3) and separately analyzed 3D-printed tablets were normalized by weight. Each sample was measured in triplicate.

2.2.4. Dissolution test conditions

A semi-automatic tablet dissolution system Sotax AT7 (Sotax AG, Aesch, Switzerland) fulfilling requirements for USP2 dissolution method was used to perform the studies. *In vitro* release profiles of the tablets (n = 3 for each infill density) were studied at 0.1 N HCl with 0.5% cetyltrimethylammonium bromide (CTAB). Each tablet was pre-weighed and placed in the vessel containing 900 ml of dissolution medium. Dissolution was carried out with a paddle speed of 100 rpm at 37 °C for 90 min. The paddle speed was then increased to 250 rpm for further 30 min to ensure full dissolution. Samples (10 ml each) were collected at time points 0, 5, 10, 15, 20, 30, 60, 90 and 120 min. The dissolution medium was replenished after each sampling with an equivalent amount of 0.5% CTAB 0.1 N HCl solution. The drug concentration of the samples was analyzed for concentration as above using Perkin Elmer Lambda 25 UV spectrophotometer at 342 nm. Expected 100% dissolution value was calculated based on the nominal value in the initial formulation blend. Dissolution profiles were visualized by plotting percentage of drug dissolved against time. At least 85% of relative dissolved drug amount (average n = 3) after 30 min was set as rapid release criteria (CDER, 1997).

2.2.5. X-ray powder diffraction (XRPD)

Powders were analyzed on a quartz sample holder. Powder blends were directly dispensed on the holder surface, 3D-printed tablets were gently/manually ground with mortar and pestle. XRPD analyses were performed on a diffractometer using a K430 X-ray generator with a copper anode (voltage: 40 kV, current: 40 mA). XRD patterns in temperature were recorded in transmission mode using quartz capillaries 1.5 mm diameter (GLASS W. Müller, Berlin, Germany). The X-ray generator was a long line focus sealed tube (Siemens; Germany, Cu anode with a Kα line at 1.54 Å, operating at voltage of 40 kV and current of 20 mA). One 2D VÅNTEC-500 Area detector (4 channels, filled with argon-ethane mixture) were used to collect the data. With the settings used, 2θ angles were calculated, ranging from 1 to 18° and from 18 to 36°. Diffractograms were generated with the software Diffrac. EVA V4.0

Table 1
Formulations compositions and process parameters (actual/measured values).

Formulation component (% w/w)	EUD_0	EUD_5	EUD_7.5	EUD_10	EUD_12.5	EUD_15	EUD_30
Lumefantrine	0.00	4.97	7.54	10.04	12.50	14.99	30.01
Eudragit E PO	75.78	72.01	70.07	68.17	66.31	64.42	53.04
Maltodextrin	10.02	9.53	9.27	9.02	8.77	8.52	7.02
Xylitol	14.19	13.49	13.12	12.77	12.42	12.07	9.93
Process parameters							
T zone 2 (°C)	43	38	39	40	40	41	40
T zone 3 (°C)	80	60	61	80	62	60	62
T zone 4 (°C)	140	120	120	100	120	120	120
T zone 5 (°C)	140	135	130	130	130	125	120
T zone 6 (°C)	140	135	130	130	130	125	120
T zone 7 (°C)	140	135	135	130	130	130	120
T zone 8 (°C)	141	135	135	131	132	130	120
T die (°C)	142	138	134	131	132	128	120
screw speed (rpm)	15	22	22	20	22	27	23
Torque (%)	17	30	33	23	28	26	35
Pressure (bar)	2	3	7	1	7	2	3
Appearance after extrusion	whitish translucid	yellow translucid	yellow translucid	yellow translucid	yellow translucid	yellow translucid	yellow opaque

from Bruker, USA.

2.2.6. Differential scanning calorimetry (DSC)

DSC measurements were performed using a Q2000 DSC (TA instrument, New Castle, PA) under nitrogen flow of 50 ml/min. Samples between 1 and 2.5 mg were analyzed using punctured aluminum pans, an empty pan was used as reference. A heating rate of 10 °C/min was set between −20 °C and 300 °C. Software Trios v4.4.1 (TA Instruments, Inc., Waters Corporation, MA, USA) was used.

2.2.7. Confocal Raman microscopy

Raman spectra were obtained with a Confocal Raman microscope (WiTec alpha 300 R, Germany). The excitation wavelength 633 nm was provided by a HeNe laser (Melles Griot, USA). Offset correction was performed for each study by calibration against silicate substrate.

Reference material spectra, including that of lumefantrine in both crystalline and amorphous states, were obtained by single spectral measurements whereby characteristic peaks for each species were defined for hyperspectral processing.

Extruded filaments and their corresponding printed tablets were embedded in epoxy resin and processed using an ultra-microtome to obtain level block cross-sections. Thereafter, cross-section surfaces were analyzed by large area scans. For printed tablets, surface scans were also performed on the ready-made tablet prior to sample cross-sectioning.

Area scans and their corresponding hyper-spectra generation were performed firstly on a large-scale, low resolution modes to gain an overview. These were 1100 × 1100 μm at 10 μm spatial resolution and 4000 × 3500 μm at 20 μm spatial resolution for the filament and printed tablets respectively. This was followed by 400 × 300 μm at 1 μm spatial resolution scans performed at two different spots for each sample. Average spectra extraction took place based on reference spectra peak evaluation performed automatically by the software. These were 1635 rel. cm^{-1} for crystalline lumefantrine, 1631 for cm^{-1} for amorphous lumefantrine, 1728 rel. cm^{-1} for Eudragit EPO, 483 cm^{-1} for maltodextrin and 1062 cm^{-1} for xylitol.

Hyperspectral data offset and baseline polynomial correction, cosmic ray removal, spectral filter application, average spectral extraction and spectral map deconvolution were performed using Witec Project FIVE 5.1 software. No artefacts by thermal effects of the laser on the samples were observed.

2.2.8. X-ray microcomputed tomography (μCT)

3D-printed tablets were evaluated in triplicate of each variant using Skyscan 1172 X-ray microtomograph (Bruker, Kontich, Belgium). Multi-projection acquisition took place at 5.93 μm resolution, 59 kV source voltage and 167 μA source current. Following the application of appropriate ring artifact and beam hardening filter, image reconstruction (tomography generation) took place using NRecon v. 1.7.3.2 software (Bruker, USA) at −0.102355 to 0.186187 attenuation coefficient (dynamic) range output. For qualitative specimen visualization, DataViewer software (Bruker, USA) was used.

Image processing and morphometry evaluation took place using ImageJ 1.52p (NIH, USA). 3D-printed tablet homographs were binarized based on pilot Renyi's entropy output (Kapur et al., 1985). Thereafter, scatter removal was performed by the application of appropriate iterations of outlier removal from the binarized tomography stacks. Inner pore extraction took place by 3D fill-hole and subtraction and, on the other hand, enclosed perimeter extraction took place by 3 iterations of multidirectional fill-hole process (Ollion et al., 2013). Solid, enclosed perimeter and pore volumes were established by voxel count whilst surface area pixel evaluation was performed using marching cubes algorithm (Lorensen and Cline, 1987). Following the development of processing and data mining sequences, all operations were carried out in an automated manner by the application of IJ1 based macros.

2.2.9. He-pycnometry

Densities of 5% LUM filaments with and without drying overnight were measured by helium pycnometry (UltraPyc 1200e; Quantachrome GmbH & Co. KG, Duisburg, Germany). For each density test ten consecutive volume measurements showing a standard deviation <0.02 cm^3 were performed with <0.07% deviation achieved. Obtained results were averaged to report 5% LUM formulation density and compare with calculated density based on X-ray μCT of 5% LUM 3D-printed tablets.

2.2.10. Data analysis

The data are presented as mean ± SD, and the differences between groups were analyzed by one-way ANOVA (MiniTab, version 17.3.1, Minitab LLC, USA) and confirmed by Fisher's test (MiniTab, version 17.3.1, Minitab LLC, USA). The statistical significance was considered at $p < 0.05$.

3. Results and discussion

3.1. Processability of hot-melt extrusion and 3D-printing

Eudragit-xylitol-maltodextrin filaments with 0–30% drug load were successfully extruded. Filaments with lumefantrine were yellowish with varying transparency as a function of drug concentration (see randomly chosen strands of the filaments in Fig. 1). Increasing concentration of active ingredient in the formulations allowed for reduction of barrel temperature with comparable extrusion speed and torque for filament production in comparison to the placebo reference (Table 1). Values of process parameters are reported here for the purpose of assuring reproducibility of the experiment while for studying the functional relationship between these parameters additional work is required.

Besides placebo, filament of the formulation with 5% drug load was the only one compatible with FDM 3D-printing due to the increased brittleness of higher drug load filaments. All further experiments were conducted with 5% lumefantrine filaments, used to manufacture tablets with 65% to 100% infill density (Fig. 2,).

3.2. Weight uniformity and morphological characteristics of 3D-printed tablets

Manufacture of lumefantrine 3D-printed tablets was achieved with size and shape being in agreement with the preset dimensions (see Table 2). Tablets with programmed infill density 80% and 100% demonstrated more uniform weight than those with 65%. Also, tablets with infill density of 80% and 100% had a very similar weight that was considerably larger than the one of tablets with 65% infill density. It should be pointed out that infill density designates only the interior while an identical outer layer (altitude shell) always exists constituting a considerable part of the weight of the tablet. Still, an effect on tablet weight was noticeable only when infill density was reduced to 65%. This demonstrates a non-linear dependence of weight as measured tablet characteristic on the programmed 3D-printing parameter. The rate and homogeneity of discharge of hot liquid mass during 3D-printing and their dependence on the porosity of the created structures might be responsible for the observed effect.

Qualitative assessment of tomography images for all specimens revealed the oval conformation of 3D-printed tablets with relatively flat top and bottom aspects (Fig. 2). A level of inner structural void demarcated by the interweaving polymer filaments was also evident. This gradually diminished especially for infill densities 80 and 100% towards the bottom of the tablet touching the hot plate likely because of material fusion. Evaluation of 3D reconstructs showed the precise multi-layered nature of the 3D-printed tablets when viewing their side aspects (3D-reconstruction, Fig. 2).

A non-destructive automated μCT morphometry analytical approach based on the application of appropriate binary threshold was developed in this study to determine surface area, solid volume, and open/close

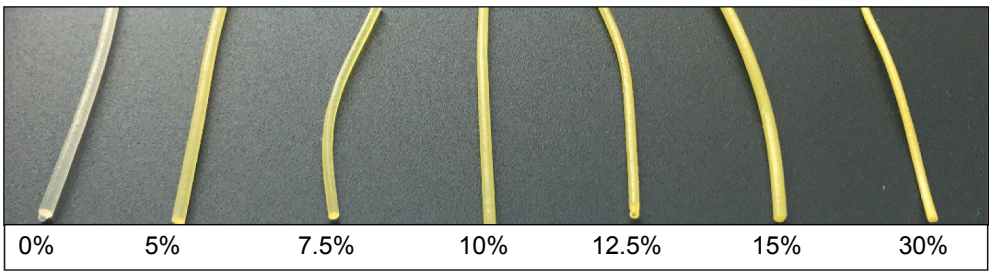

Fig. 1. Photographs of Eudragit E PO-based filaments with 5 to 30% lumefantrine following hot-melt extrusion. Approximate length of the shown filaments is 5 cm.

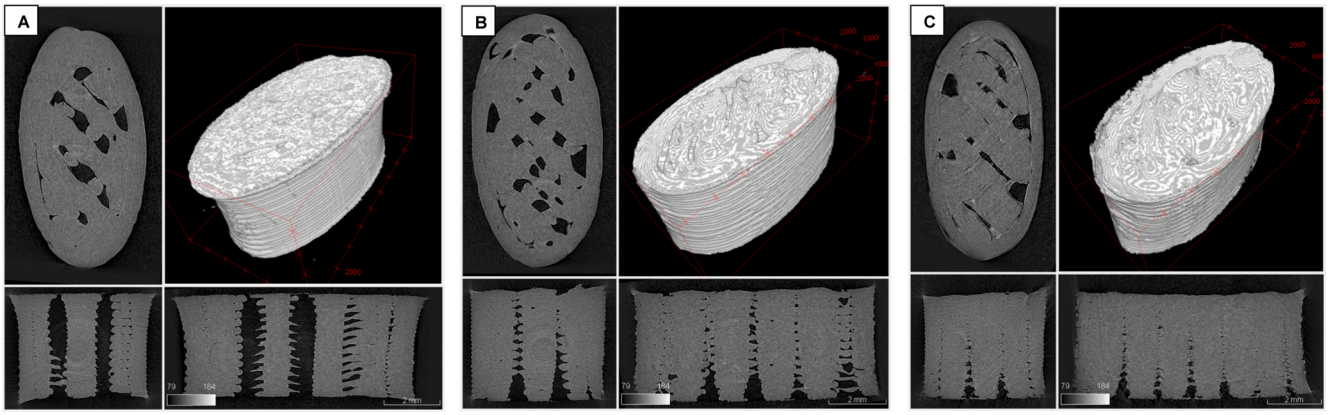

Fig. 2. X-ray micro-CT images of 5% lumefantrine 3D-printed tablets with (A) 65%, (B) 80% and (C) 100% infill density. Top left of each panel is cross-section perpendicular to z axis, bottom-left and bottom right of each panel are cross-sections parallel to the z axis of the tablet in x and y direction, respectively. Top right of each panel shows the reconstructed view of the 3D-printed tablet. 3D-reconstruction and the cross-sections, where applicable, are shown upside-down, the top plane corresponding to the bottom of 3D-printed tablet.

Table 2
Morphological characteristics of 5% lumefantrine 3D-printed tablets.

Programmed infill density	Weight** (mg)	x dimension* (mm)	y dimension* (mm)	z dimension* (mm)	Surface area* (mm^2)	Closed pore volume* (mm^3)	Open pore volume*(mm^3)	Measured relative density*
65%	108 ± 2	9.2 ± 0.3	4.9 ± 0.1	3.9 ± 0.05	422.9 ± 5.4	0.08 ± 0.02	13.96 ± 0.40	0.8 ± 0.007
80%	142 ± 1	8.9 ± 0.2	4.5 ± 0.1	4.0 ± 0.01	316.9 ± 39.5	0.48 ± 0.09	4.80 ± 2.06	0.925 ± 0.031
100%	139 ± 1	9.2 ± 0.3	4.9 ± 0.1	3.9 ± 0.05	291.8 ± 43.8	0.29 ± 0.09	3.33 ± 1.72	0.943 ± 0.028

Data presented as mean ± std, based on average of *n = 3 or **n = 6.

pores volume of 3D-printed tablets. The density values established by correlating solid volume of specimens with their weight yielded an average of 1.19 ± 0.032 g/cm^3 (11 tablets with 3 infill densities 3D-printed from formulation 5% lumefantrine, 72% Eudragit E PO, 13.5% xylitol, 9.5% maltodextrin). This was in full agreement to measured filament density by He-pycnometry of 1.19 ± 0.011 g/cm^3 for the same formulation validating the results provided by the μCT technique.

Absolute and specific surface area and accessible porosity of tablets were significantly larger for 65% infill density than for 80% and 100% infill density (Fig. 3). Apparently, the higher the density of deposition, the more confluence between the deposited strands takes place leading to less exposed surface area. Tablets with 80% and 100% programmed infill density showed similar morphological characteristics, surface area and open pore volume being slightly larger for the former than for the latter, this difference being statistically not significant. The outer layer that is identical for all infill densities and occupies considerable part of the tablet volume and lowers the effect of programmed infill density on actual porosity may be partly responsible for this result. Interestingly, however, infill density of 65% produced tablets with significantly different morphological characteristics while no big differences between tablets with 80% and 100% infill density were observed. These results of morphological characteristics for tablets of different design are consistent with the results of tablet weight discussed above. Hence, increased infill density between 65 and 80% resulted in the deposition of more material which however led to smaller exposed surface area likely due to confluence of 3D-printed strands eliciting, in turn, a reduced open pore volume. This trend is not evident above 80% infill density. Enclosed pore volume seemed to be larger for 80% and 100% than for 65% infill density (Fig. 3), no clear ordering, however, is evident. The present data therefore show that programmed structural characteristics influence the morphology of 3D-printed tablets in a foreseeable fashion only within a certain value range. For a complete understanding of the correlation between programmed and actual characteristics of manufactured objects and a control of the 3D-printing process, further studies addressing, among others, the rheologic behavior of the hot fluid mass under process conditions are required.

Measured relative density (V_{solid}/V_{total}) of the 3D-printed tablets was found to be 0.8 for 65% infill density and slightly above 0.9 for both 80% and 100% infill densities. Notably, measured density was markedly higher than programmed density except for 100% designed infill in agreement with the above discussion about other morphological characteristics. Due to grid design and the omission of top and bottom solid layer, actual available surface area was higher than reported previously for cylinder-shaped FDM tablets with smaller size (Goyanes et al., 2015).

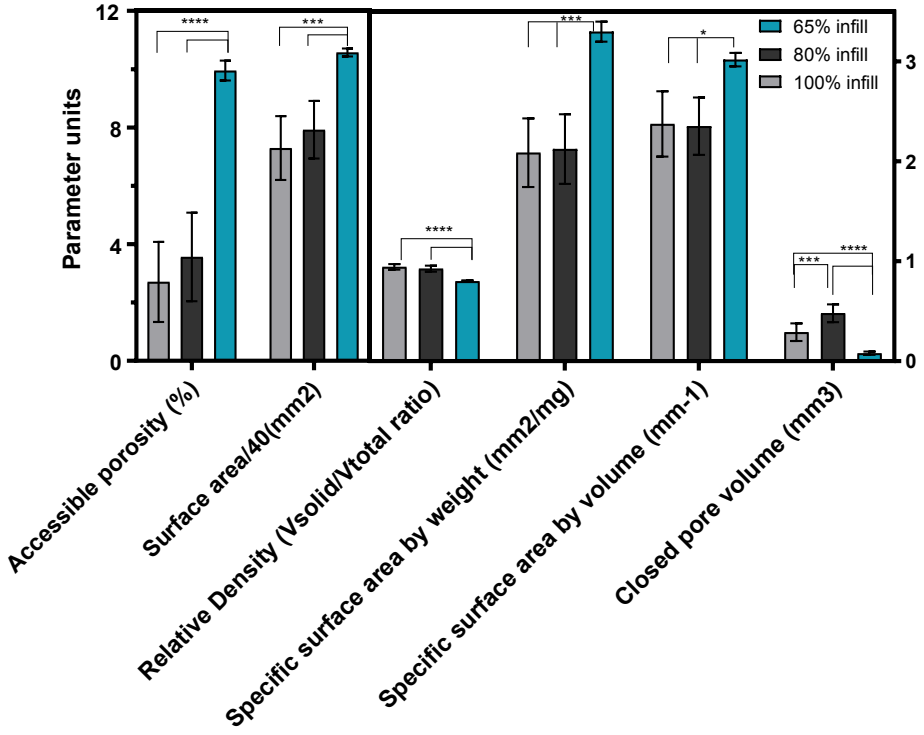

Fig. 3. Morphological characteristics of 3D-printed 5% lumefantrine tablets for three infill densities. Values on left and right y-axis correspond to columns left and right of the black vertical line, respectively. ****p < 0.0001, ***p < 0.001, **p < 0.01, *p < 0.05.

3.3. Drug content and degradation products

Lumefantrine appeared to degrade during hot-melt extrusion (no stabilizer/anti-oxidant was added), resulting in 92–97.5% assay depending on drug load and process parameters (Table 3). Decreasing HME temperature from 138 °C to 120 °C for higher loads of lumefantrine resulted in values that were closer to nominal in 7-month-old filaments. For the FDM-processable formulation, assay and by-/degradation product (BDP) values in filaments and 3D-printed tablets analyzed 2 months after manufacture were similar, demonstrating no additional degradation during FDM 3D-printing process.

3.4. Solid state analysis

DSC analysis showed a melting temperature of about 130 °C for pure drug, with absence of a melting peak for lumefantrine in physical powder blends, filaments, and 3D-printed tablets with 5% drug (Fig. 4A). This lack of melting peak might be attributed to dissolution of lumefantrine in molten Eudragit EPO or peak below limit of detection due to low concentration of drug in the formulation. No melting peak characteristic to crystalline drug was observed for up to 12.5% lumefantrine in physical powder blends and filaments (Fig. S1B), with a weak peak around 130 °C appearing only when drug concentration was increased to 30% (Fig. S1A), which is in line with the proposed explanations. XRPD analysis of 5% lumefantrine 3D-printed tablets and filaments with up to 12.5% drug content did not show diffraction peaks suggesting that the drug was present in the amorphous state, as opposed to the physical powder blends showing diffraction peaks at 18°,19°,20° and 23° 2θ which are characteristic to pure crystalline lumefantrine (Fig. 4B, Fig. S1B). For filaments with drug load of 30% drug crystalline content was visible in the XRPD (Fig. S1A).

Confocal Raman microscopy mapping confirmed that lumefantrine was fully amorphous in 5% drug load 3D-printed tablets (Fig. 5A,B). This was independent of the infill density. In filaments including those with 5% drug load the presence of crystalline lumefantrine (characteristic peaks within 1634–1636 cm^{-1}) was detected in Raman (Fig. 5D,E). This is in contrast to XRPD measurements in which drug crystallinity was undetectable in the filaments at low drug load. Raman analysis also demonstrated crystallinity for all filaments with higher drug load (Fig. 5E,F) in agreement with XRPD data for filament with 30% lumefantrine load. Eudragit EPO was fully miscible with lumefantrine in the amorphous solid state and the two substances were not detected as individual entities (Fig. 5A–E). For 30% lumefantrine filament (Fig. 5F) orange color corresponding to the amorphous matrix was not visible due

Table 3
Assay and degradation products in selected lumefantrine formulations.

Product type	Drug load (%)	Assay (%)	BDP1 (% product)	BDP2 (% product)	BDP3 (% product)	HME temperature (°C)	3D-printing temperature (°C)	Age (months)
Filament	5	92.2 ± 0.11	not detected	0.42 ± 0.02	0.11 ± 0.12	138	n.a.	7
Filament	15	96.7 ± 0.77	0.14 ± 0.005	0.50 ± 0.02	0.16 ± 0.001	128	n.a.	7
Filaments	30	97.5 ± 0.02	0.20 ± 0.005	0.87 ± 0.02	0.16 ± 0.02	120	n.a.	7
3D-printed tablet	5	93.1 ± 0.34	not detected	0.26 ± 0.24	0.07 ± 0.05	138	160	2*

*3D-printed from 5-months old filaments.

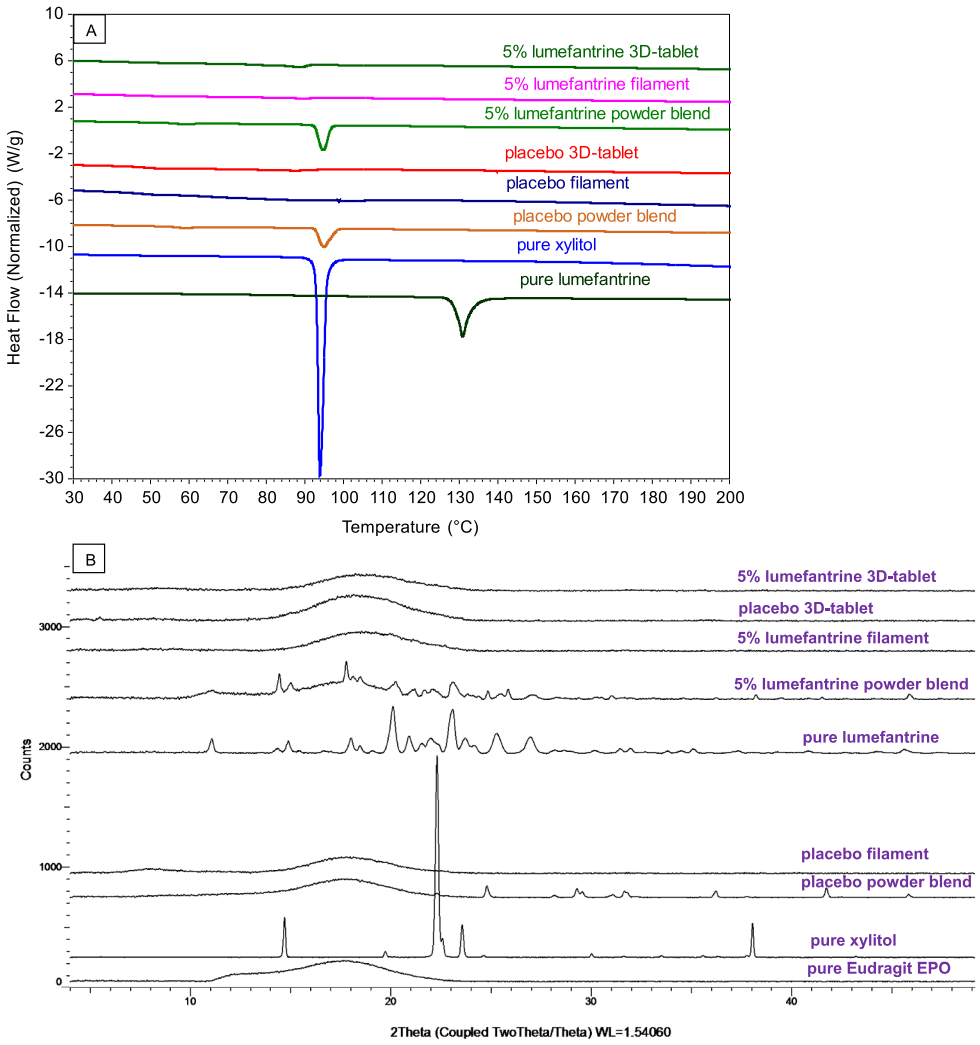

Fig. 4. (A) DSC thermograms and (B) XRPD diffractograms of 5% lumefantrine formulation (5% lumefantrine: 72% Eudragit E PO: 13.5% xylitol: 9.5% maltodextrin) and corresponding placebo throughout manufacturing steps from powder blends to 3D-printed tablets.

to its weaker signal-to-noise ratio compared to the crystals, as crystals have much better scattering properties than amorphous material or polymer and therefore the signal of concentrated crystals was significantly stronger than of the amorphous matrix.

Interestingly, 3D-printed tablets with 5% lumefantrine showed no drug crystallinity by Raman micro-spectroscopy and by XRPD analysis while the corresponding filament exhibited drug crystallinity by Raman but not by XRPD. All samples were stored at room temperature before analysis. The tablets were analyzed by Raman 16 weeks after manufacture and the filaments were analyzed 10–30 weeks after manufacture by Raman and 8 weeks after manufacture by XRPD. The obtained results can therefore be explained by assuming that crystallinity was present in the filaments at the low drug content of 5% but not detected by XRPD because of a high limit of detection or that the drug was in an amorphous state in the filaments at the time of XRPD analysis and crystallized by the time Raman analysis was performed (8 versus 10 to 30 weeks, respectively). Incidentally, the delayed Raman analysis is because this technique is quite time-consuming. Hence, it is theoretically possible that at the time of tablet manufacture by 3D-printing the used filaments contained the drug either in a crystalline or an amorphous state. The former case, if true, would entail transformation of crystalline to amorphous drug through the process of 3D-printing being in essence a hot-melt process, and would be interesting to further investigate. Significantly, the drug was present in the tablets in an amorphous state for up to 16 weeks after manufacture. Regardless of whether this amorphization was achieved in the process of 3D-printing or the drug was in an amorphous state in the filament at the time of 3D-printing, this process illustrates an interesting option to make amorphous solid dispersions during decentralized 3D-printing. While drug crystallization in the 3D-printed tablets may occur upon longer storage (currently 16 weeks versus a maximum of 30 weeks for the filaments), the determined stability of the amorphous state is considered to be sufficient for practical purposes in the context of decentralized manufacturing followed by on-site administration.

These findings highlight the importance of using sensitive techniques (i.e., Raman micro-spectroscopy versus XRPD) for crystallinity determination that is critical for *in-vivo* bioavailability of BCS class IV compounds. The development of robust processes requires testing of intermediate products such as filaments as well as of the final 3D-printed tablets for the amorphous form of lumefantrine, which is an enabling formulation type (Jain et al., 2017; Jain et al., 2018). Lumefantrine was found to be fully amorphous in the 3D-printed drug product with 5% drug load 16 weeks after production, which could be promising for decentralized production and reduction of risk of recrystallization upon storage in comparison to traditional amorphous solid dispersion dosage forms.

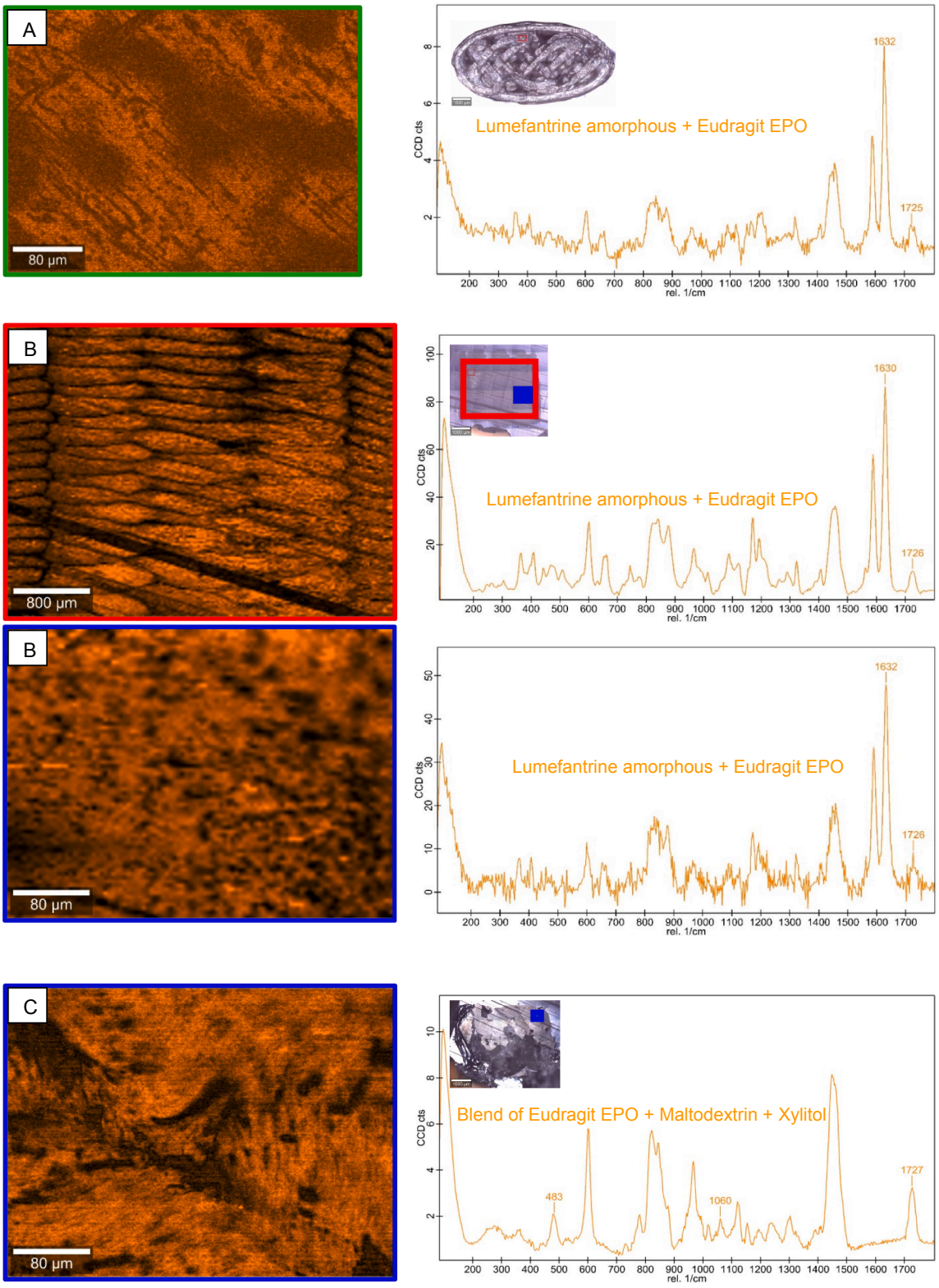

Fig. 5. Raman spectral map (left hand-side panels) and extracted spectra including representative reflection optical micrograph (right hand side panels) for: (A) surface of 5% lumefantrine 3D-printed tablet; (B) cross-sections of 5% lumefantrine 3D-printed tablet at low and high magnification, (C) corresponding placebo tablet, (D) 5% low and high magnification, (E) 15% and (F) 30% lumefantrine filament cross-sections. Crystalline lumefantrine is shown in blue, amorphous lumefantrine is shown in orange. Images (A), (B), (C) are typical of all infill densities.

3.5. Dissolution studies and morphology-dissolution relationship

Dissolution results of 3D-printed tablets with 5% lumefantrine and three different infill densities in 0.1 N HCl with 0.5% CTAB are shown in Fig. 6. The use of dissolution medium with the addition of surfactant is recommended for testing of IR drug products containing insoluble or

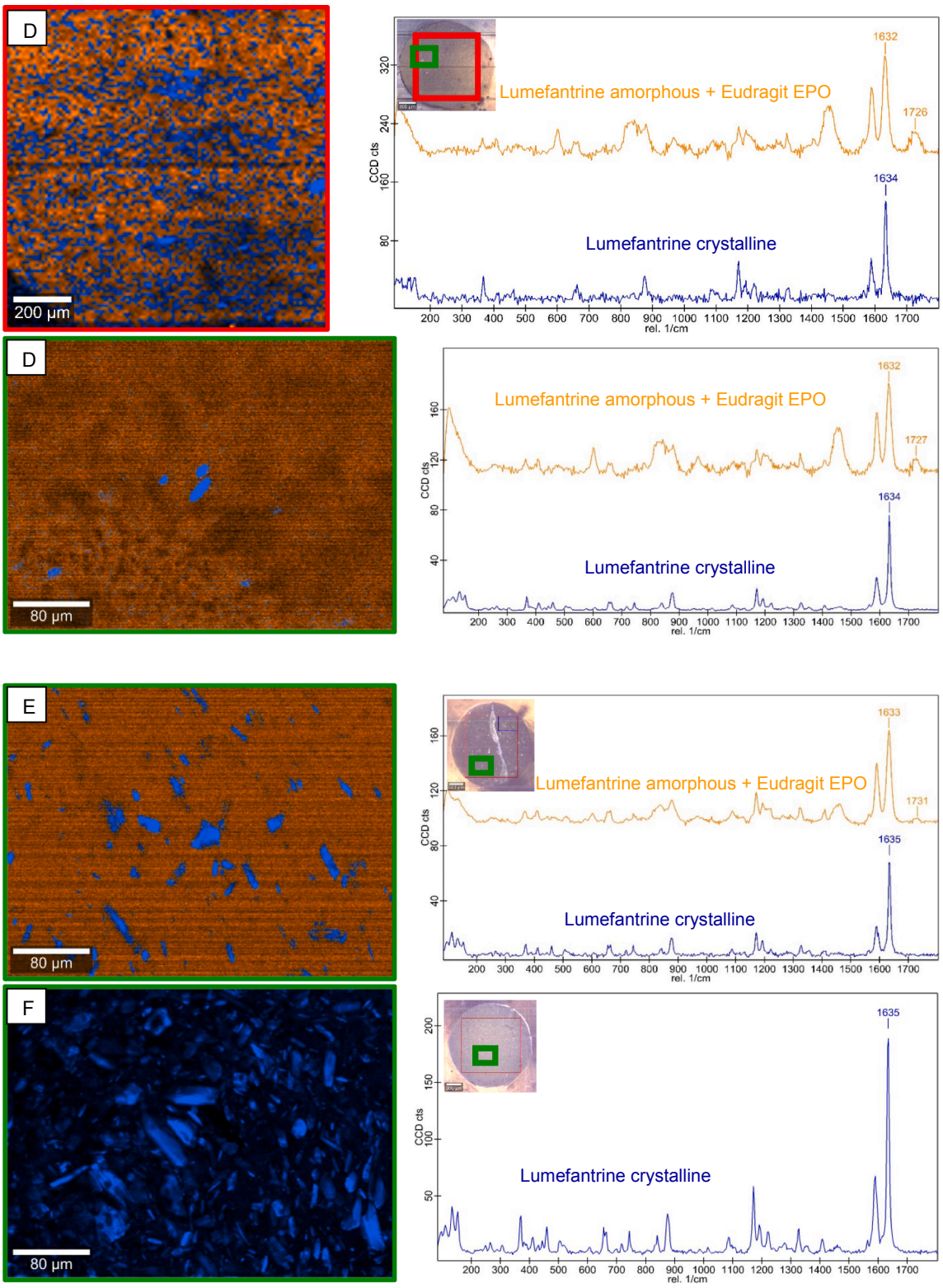

Fig. 5. (*continued*).

sparingly water-soluble APIs (CDER, 1997). Tablets with 65% infill density demonstrated rapid dissolution as about 90% of the drug was released in 30 min. Hence, formulating lumefantrine with Eudragit EPO as primary matrix former and a combination of xylitol with maltodextrin was demonstrated as promising approach for FDM to achieve immediate release of this model BCS class IV compound. Increase in infill density to 80% resulted in slower API release with about 78% dissolving in 30 min, and still further decrease of release rate was found for 100% infill density (about 69% dissolved after 30 min). Complete lumefantrine dissolution from 65% and 80% infill densities occurred at 60 min time point, however for 100% infill density full dissolution occurred at 120 min only. Tablet designs with 80% and 100% infill density, therefore, exhibited lower dissolution rate and would not meet the strictest criteria set by the FDA recommendation for immediate release products (CDER,

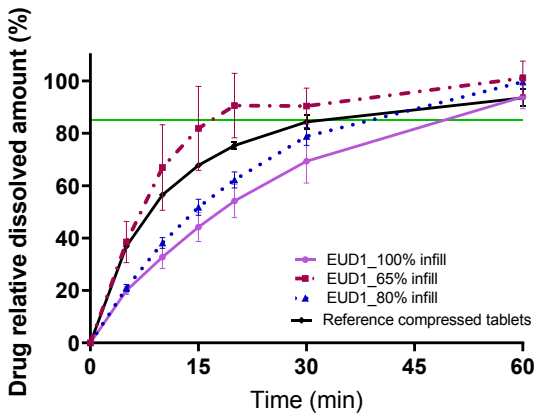

Fig. 6. Dissolution profiles of 3D-printed tablets (5% lumefantrine, 72% Eudragit E PO, 13.5% xylitol, 9.5% maltodextrin) with 100%, 65% and 80% infill density; and of reference compressed 120 mg lumefantrine tablets. Points and bars depict mean and standard deviation of n = 3 measurements.

1997). Release rate was statistically significantly higher for 65% infill density than for 80 and 100% (Fig. 7). The faster drug release from the lower infill density tablets correlates with the significantly higher specific surface area and accessible porosity found for these tablets (Fig. 7). This effect of infill density is in agreement with previous findings (Alhnan, 2017; Solanki et al., 2018). The fact that infill density and porosity of the tablets affected the drug dissolution rate suggests that water penetrated freely through the pores of FDM 3D-printed lumefantrine tablets. No influence of enclosed volume on dissolution rate is evident as might be expected. Relative drug amount dissolved as a function of time from reference compressed tablets was somewhat higher than the result of 3D-printed tablets with 80% and 100% infill density but lower than the result of 3D-printed tablets with 65% infill density (Fig. 6). Since the reference tablets are marketed as immediate release product, these data strongly suggest that the low infill density tablets manufactured by FDM 3D-printing also fulfill this classification. It should be noted, however, that the used dissolution medium raises no claim of biorelevance and that it is not discriminating with respect to dissolution rate of crystalline versus amorphous drug substance. Nevertheless, existing evidence indicates that amorphous solid dispersion of drug (as that comprising the 3D-printed tablets) provides higher bioavailability *in vivo* (Jain et al., 2017; Jain et al., 2018) than crystalline drug (which is contained in the reference tablets). Therefore, the low infill density 3D-printed tablets could be expected to exhibit higher bioavailability than the commercial tablets.

These data clearly demonstrate that tablet morphology produced by design with the 3D-printing process can be used to modulate drug dissolution rate and is crucial for achieving immediate release characteristics. Morphological characteristics of tablets in terms of exposed surface area and accessible pore volume are shown to closely correlate with dissolution rate in a mechanistically predictable fashion. Thus, the lumefantrine-Eudragit EPO system was responsive to an increase in surface area and porosity that allowed greater water access and faster dissolution. Programmed structural properties were reflected in tablet characteristics illustrating a link between manufacture and performance in fused deposition modeling. However, the relationship between infill density and surface area and porosity was not linear and must be further investigated. Notably, 3D-printed tablets with 65% infill density were the only variant that showed statistically significant increase in surface area, accessible porosity, and specific surface area by weight and by volume, as well as decrease in relative density, while tablets with 80% and 100% infill density did not differ significantly.

This work, then, illustrates the potential of additive manufacturing for tailoring performance characteristics of pharmaceuticals. Achieving immediate release properties of a poorly water-soluble BCS class IV compound by FDM has not been reported to the best of the authors' knowledge before.

4. Conclusions

Immediate release Eudragit EPO-based 3D-printed tablets with BCS class IV model compound were successfully developed via structural design modification. Incorporation of programmed infill density of 65%, was needed to meet rapid release criteria (at least 85% drug dissolved

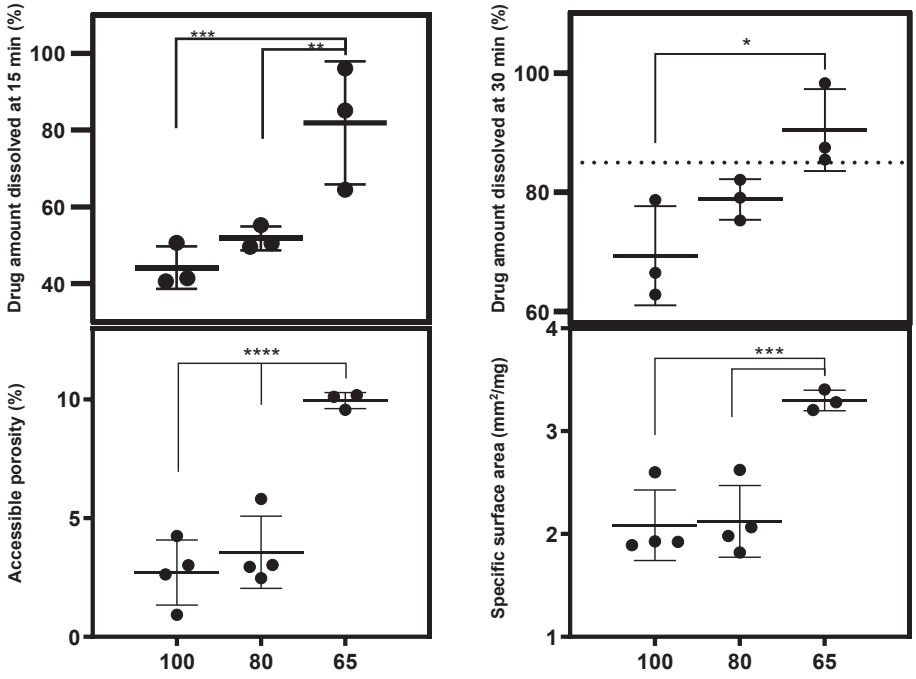

Fig. 7. Statistical analysis of morphological characteristics and dissolution performance of 3D-printed 5% lumefantrine tablets for three infill densities shown in the x-axis, *P < 0.05, **P < 0.01, ***P < 0.001, ****P < 0.0001.

after 30 min). Moreover, fully amorphous solid dispersion as detected by highly sensitive Raman mapping was achieved via 3D-printing which was stable for a time reasonable for decentralized manufacturing. Tablets with drug load of 5% were printed while for higher drug load no 3D-printing was possible because of increased brittleness of filaments.

The observed weight deviation points out the need for further understanding and development of pharmaceutical FDM 3D-printing process, as well as better control of temperature tolerances. Additional formulation development following adaptation of 3D-printing equipment (such as nozzles and gear wheels) might be required to obtain tablets with the weight uniformity meeting regulatory requirements. Also, formulation modification to achieve higher drug load should be pursued. Ultimately, addition of chemical stabilizer/antioxidant for this API should be considered and palatability studies of the dosage form should be performed.

The developed non-destructive μCT-based analytical methodology provided accurate morphological quantification of 3D-printed tablets, which was linked to dissolution behavior. Accessible porosity, surface area, relative density, and specific surface area by weight and by volume were identified as significant parameters responsible for dissolution rate acceleration in the 65% infill density tablets. Similar morphological characteristics between 80% and 100% infill densities were reflected in dissolution performance. For the future development of IR FDM-printed dosage forms one could reduce closed pores volume, embrace open pores, as well as optimize balance between shape/size and dissolution. With regards to IR dosage forms with poorly-water-soluble compounds, combinational approach of formulation, process and morphology might be required.

Understanding of formulation critical design and quality attributes could facilitate dose and release profile adjustments of solid dosage forms according to patient needs. This could pave the way to a new paradigm of decentralized manufacturing at hospital and community pharmacy, where one filament could be a drug formulation to deliver a range of dosage strengths and release profiles.

CRediT authorship contribution statement

Marina Fanous: Investigation, Methodology, Writing - original draft. **Malak Bitar:** Methodology. **Sarah Gold:** Resources, Conceptualization, Supervision. **Adam Sobczuk:** Methodology. **Stefan Hirsch:** Resources, Conceptualization, Supervision. **Joerg Ogorka:** Funding acquisition, Project administration. **Georgios Imanidis:** Writing - review & editing, Supervision.

Declaration of Competing Interest

The authors declare the following financial interests/personal relationships which may be considered as potential competing interests: M.B., S.G., S.H. and J.O. are employees of Novartis Pharma AG. A.S. is a contractor providing services to Novartis Pharma AG and employed by Hays AG. M.F. is PhD student at the University of Basel and is funded by Novartis Pharma.

Acknowledgements

Authors would like to thank Eric Brech, Allain Moyon, Christophe Nivill, Armin Katzenstein, Pascal Haener, Mai-Loan Nguyen and Hakan Topak for analytical support in the study, and Severine Serreau and Hubert Ferry for the assistance in hot-melt extrusion. Scientific discussions with Allan MacLean, Edgar John, Flavio Fabiani and James Pazdan are highly appreciated.

Funding sources

This research did not receive any specific grant from funding agencies in the public, commercial, or not-for-profit sectors other than the affiliations of the authors.

Appendix A. Supplementary material

Supplementary data to this article can be found online at https://doi.org/10.1016/j.ijpharm.2021.120417.

References

Alhnan, M., 2017. Solid forms and methods of preparing the same WO 2017/072536 A1.
Alhnan, M., Okwuosa, T.C., Sadia, Muzna, W.K., Ahmed, W., Arafat, B., 2016. Emergence of 3D printed dosage forms: opportunities and challenges. Pharmac. Res. 33, 1817–1832.
Arafat, B., Wojsz, M., Isreb, A., Forbes, R.T., Isreb, M., Ahmed, W., Arafat, T., Alhnan, M. A., 2018. Tablet fragmentation without a disintegrant: A novel design approach for accelerating disintegration and drug release from 3D printed cellulosic tablets. Eur. J. Pharmac. Sci. 11, 191–199.
Awad, A.F.F., Trenfield, S.J., Patel, P., Goyanes, A., Gaisford, S., Basit, A.W., 2019. 3D printed pellets (miniprintlets): a novel, multi-drug, controlled release platform technology. Pharmaceutics 11, 148.
Awad, A.Y.A., Trenfield, S.J., Goyanes, A., Gaisford, S., Basit, A.W., 2020. 3D printed tablets (printlets) with braille and moon patterns for visually impaired patients. Pharmaceutics 12, 172.
Azad, M.A.O.D., Kimbell, G., Badruddoza, A.Z.M., Hossain, M.S., Sultana, T., 2020. Polymers for extrusion-based 3D printing of pharmaceuticals: a holistic materials-process perspective. Pharmaceutics 12, E124.
Boyd, B., Bergström, C.A.S., Vinarov, Z., Kuentz, M., Brouwers, J., Augustijns, P., Brandl, M., Bernkop-Schnürch, A., Shrestha, N., Préat, V., Müllertz, A., Bauer-Brandl, A., Jannin, V., 2019. Successful oral delivery of poorly water-soluble drugs both depends on the intraluminal behavior of drugs and of appropriate advanced drug delivery systems. Eur. J. Pharmac. Sci. 137, 104967.
Butler, J.M.D.J., 2010. The developability classification system: application of biopharmaceutics concepts to formulation development. J. Pharm. Sci. 99, 4940–4954.
CDER, 1997. Dissolution Testing of Immediate Release Solid Oral Dosage Forms Guidance for Industry. In: U.S. Department of Health and Human Services, F.a.D.A. (Ed.), U.S. Government Printing Office: Washington, DC.
Curti, C.K.D., Russell, C.A., 2020. Current formulation approaches in design and development of solid oral dosage forms through three-dimensional printing. Prog. Addit. Manuf. 5, 111–123.
Fanous, M., Gold, S., Hirsch, S., Ogorka, J., Imanidis, G., 2020a. Development of Immediate Release (IR) 3D-printed oral dosage forms with focus on industrial relevance. Eur. J. Pharmac. Sci. 155, 105558.
Fanous, M., Gold, S., Muller, S., Hirsch, S., Ogorka, J., Imanidis, G., 2020b. Simplification of fused deposition modeling 3D-printing paradigm: feasibility of 1-step direct powder printing for immediate release dosage form production. Int. J. Pharmac. 578, 119124.
GBIResearch, 2012. Oral drug delivery market report, http://www.gbiresearch.com/, last retrieved 07th August 2020.
Goyanes, A., Buanz, A.B., Hatton, G.B., Gaisford, S., Basit, A.W., 2014a. 3D printing of modified-release aminosalicylate (4-ASA and 5-ASA) tablets. Eur. J. Pharmac. Biopharmac. 89, 157–162.
Goyanes, A., Buanz, A.B.M., Basit, A.W., Gaisford, S., 2014b. Fused-filament 3D printing (3DP) for fabrication of tablets. Int. J. Pharmac. 476, 88–92.
Goyanes, A., Kobayashi, M., Martínez-Pacheco, R., Gaisford, S., Basit, A.W., 2016. Fused-filament 3D printing of drug products: Microstructure analysis and drug release characteristics of PVA-based caplets. Int. J. Pharm. 514, 290–295.
Goyanes, A., Martinez, P.R., Basit, Buanz, A.W., Gaisford, S., 2015. Effect of geometry on drug release from 3D printed tablets. Int. J. Pharmac. 494, 657–663.
Ilyés, K., Kovács, N.K., Balogh, A., Borbás, E., Farkas, B., Casian, T., Marosi, G., Tomuță, I., Nagy, Z.K., 2019. The applicability of pharmaceutical polymeric blends for the fused deposition modelling (FDM) 3D technique: material considerations–printability–process modulation, with consecutive effects on in vitro release, stability and degradation. Eur. J. Pharmac. Sci. 129, 110–123.
Jain, J., Leong, F.J., Chen, L., Kalluri, S., Koradia, V., Stein, D.S., Wolf, M.-C., Sunkara, G., Kota, J., 2017. Bioavailability of lumefantrine is significantly enhanced with a novel formulation approach, an outcome from a randomized, open-label pharmacokinetic study in healthy volunteers. Antimicrob. Agents Chemother. 61, e00868–00817.
Jain, J., Leong, F.J., Winnips, C., Wolf, M.-C., 2018. Therapeutic regimen. In: 20180303837 (Ed.), Patent Application A61K 31/522 (20060101); A61P 33/06 (20060101); ed.
Kapur, N., Sahoo, P.K., Wong, A.K.C., 1985. A new method for gray-level picture thresholding using the entropy of the histogram. Comput. Vis. Graph. Image Process. 29, 273–285.
Kawabata, Y., Wada, K., Nakatani, M., Yamada, S., Onoue, S., 2011. Formulation design for poorly water-soluble drugs based on biopharmaceutics classification system: basic approaches. Int. J. Pharm. 420, 1–10.
Korte, C.a.Q.J., 2018. 3D-printed network structures as controlled-release drug delivery systems: dose adjustment, API release analysis and prediction. AAPS PharmSciTech 19, 3333.
Kyobula, M., Adedeji, A., Alexander, M.R., Saleh, E., Wildman, R., Ashcroft, I., Gellert, P. R., Roberts, C.J., 2017. 3D inkjet printing of tablets exploiting bespoke complex

geometries for controlled and tuneable drug release. J. Control. Release 261, 207–215.
Lobenberg, R.A.G., 2000. Modern bioavailability, bioequivalence and biopharmaceutics classification system. New scientific approaches to international regulatory standards. Eur. J. Pharmac. Biopharmac. 50, 3–12.
Lorensen, W., Cline, H.E., 1987. Marching cubes: a high resolution 3D surface construction algorithm. ACM SIGGRAPH Comput. Graph. 21, 163–169.
Marketsandmarkets, 2013. Drug delivery technology market. https://www.marketsandmarkets.com/ResearchInsight/drug-delivery-technologies-market.asp.
Meier, C., Nollenberger, N., Gryczke, A., Petereit, H.-U., Dressman, J., 2008. Pharmaceutical compositions containing mixtures of polymers and active agents poorly soluble in water A61K9/2027 ed. Evonik Roehm GmbH.
NHS, 2016. Improving outcomes through personalized medicine, https://www.england.nhs.uk/wp-content/uploads/2016/09/improving-outcomes-personalised-medicine.pdf.
Norman, J., Madurawe, R.D., Moore, C.M.V., Khan, M.A., Khairuzzaman, A., 2017. A new chapter in pharmaceutical manufacturing: 3D-printed drug products. Adv. Drug Deliv. Rev. 108, 39–50.
Ollion, J., Cochennec, J., Loll, F., Escudé, C., Boudier, T., 2013. TANGO: a generic tool for high-throughput 3D image analysis for studying nuclear organization. Bioinformatics 29, 1840–1841.
Pietrzak, K., Isreb, A., Alhnan, M.A., 2015. A flexible-dose dispenser for immediate and extended release 3D printed tablets. Eur. J. Pharm. Biopharm. 96, 380–387.
Puri, V., Brancazio, D., Desai, P.M., Jensen, K.D., Chun, J.H., Myerson, A.S., Trout, B.L., 2017. Development of maltodextrin-based immediate-release tablets using an integrated twin-screw hot-melt extrusion and injection-molding continuous manufacturing process. J. Pharm. Sci. 106, 3328–3336.
Rycerz, K.S.K., Czapiewska, M., Arafat, B.T., Habashy, R., Isreb, A., Peak, M., Alhnan, M. A., 2019. Embedded 3D printing of novel bespoke soft dosage form concept for pediatrics. Pharmaceutics 11, 630.
Sadia, M.A.B., Ahmed, W., Forbes, R.T., Alhnan, M.A., 2018. Channelled tablets: an innovative approach to accelerating drug release from 3D printed tablets. J. Control Release 269, 355–363.
Sadia, M., Sośnicka, A., Arafat, B., Isreb, A., Ahmed, W., Kelarakis, A., Alhnan, M.A., 2016. Adaptation of pharmaceutical excipients to FDM 3D printing for the fabrication of patient-tailored immediate release tablets. Int. J. Pharm. 513, 659–668.
Solanki, N., Tahsin, M., Shah, A.V., Serajuddin, A.T.M., 2018. Formulation of 3D printed tablet for rapid drug release by fused deposition modeling: screening polymers for drug release, drug-polymer miscibility and printability. J. Pharm. Sci. 107, 390–401.
Song, Y.Z.D., Chen, X., Su, Z., Nie, H., Lubach, J.W., Smith, D., Byrn, S., Pinal, R., 2016. Acid-base interactions in amorphous solid dispersions of lumefantrine prepared by spray-drying and hot-melt extrusion using X-ray photoelectron spectroscopy. Int. J. Pharmac. 514, 456–464.
Trenfield, S., Awad, A., Goyanes, A., Gaisford, S., Basit, A.W., 2018. 3D printing pharmaceuticals: drug development to frontline care. Trends Pharmacol. Sci. 39, 440–451.
Vogenberg, F., Isaacson Barash, C., Pursel, M., 2010. Personalized medicine: part 1: evolution and development into theranostics. P & T 35, 560–576.
Wei, C.S.N., Vasoya, J.M., Shah, A.V., Serajuddin, A.T.M., 2020. Development of 3D printed tablets by fused deposition modeling using polyvinyl alcohol as polymeric matrix for rapid drug release. J. Pharmac. Sci.
Zema, L., Melocchi, A., Maroni, A., Gazzaniga, A., 2017. Three-Dimensional printing of medicinal products and the challenge of personalized therapy. J. Pharm. Sci. 106, 1697–1705.